Journal of the European Ceramic Society **19** (1999) 2067–2072

PII: S0955-2219(99)00020-5
0955-2219/99/$ - see front matter

Direct Microwave Sintering of Yttria-stabilized Zirconia at 2·45 GHz

A. Goldstein,[a]* N. Travitzky,[b] A. Singurindy[a] and M. Kravchik[a]

[a]Israel Ceramic and Silicate Institute, Technion City, Haifa 32000, Israel
[b]Department of Solid Mechanics, Materials and Structures, Tel Aviv University, Tel-Aviv, Israel

(Received 1 September 1998; accepted 22 January 1999)

Abstract

The feasibility of using direct MW heating—with 2·45 GHz radiation distributed in multimode applicators—for the obtainment of uncracked fully dense zirconia ceramics was studied. It was found that such a sintering approach can be used in the case of $ZrO_2(Y_2O_3)$ powder compacts. Suitable correlation between target load mass, heating chamber architecture and forward power profile is the key to direct MW heating without thermal runaway. Sintered bulk densities close to the theoretical were obtained after firing cycles of about 2 h. Sintering rate enhancement in the MW furnace resulted in a reduction of ~100°C in the minimal temperature required for full densification. Mechanical properties of MW and conventionally sintered specimens (fully dense state) were not significantly different. © *1999 Elsevier Science Limited. All rights reserved*

Keywords: microwave processing, ZrO_2, sintering, mechanical properties, microstructure-final.

1 Introduction

Sintering of zirconia ceramics—based on their interaction with microwaves (MW) of various frequency (2·45–60 GHz range)—has been previously studied.[1–14] For the case of 2·45 GHz radiation in *multimode applicators*—currently the configuration with the best prospects for industrial scale use—all the systematic research has been performed using the *susceptor assisted MW heating* (MW–SAH) approach. The presence of susceptors modifies the electromagnetic field distribution and its mean intensity, introduces heat sources external to the specimens and may shield, to some extent, the target load from the field.[15] In such conditions the heating of the specimens takes place in a way different from that encountered when *direct MW heating, without susceptor* (MW–HWS), is used. In MW–SAH potential nonthermal MW effects may be reduced or eliminated and this approach is also less convenient for industry. Considering the above, it seems that a more thorough investigation of the MW–HWS approach, as a means for the densification of zirconia powder compacts, is of both scientific and technological interest.

In this work the densification of a TZP type material $ZrO_2(Y_2O_3)$ by the MW–HWS approach was studied. The densification levels, microstructures and mechanical properties obtained were compared to those received after heating in a resistive 'conventional' furnace (CFH) approach. The influence of factors like specimen size and shape, green density uniformity and the nature of the firing atmosphere on the MW sintering process was also investigated.

2 Experimental

2.1 Materials

An yttria (5·17 wt%) stabilized, TZP type commercial zirconia powder, grade HSY 3·0U of DKKKK, Japan, was used.

The zirconia crystallites were agglomerated in multilevel aggregates with a size $\geq 0{\cdot}2\,\mu$m; the first and second level strong aggregates were spheroidal in shape. The material exhibits a specific surface area of $22\,m^2\,g^{-1}$. The only 'high' concentration impurity is alumina, 0·7 wt%. The as-received material contains some 25 wt% monoclinic phase, the remainder being tetragonal. In accord with the phase diagram of the ZrO_2–$YO_{1.5}$ system,[16] the X-ray diffraction (XRD) pattern [(004) and (400) peaks; $2\theta = 73$–$75°$ region], indicates that no cubic material is present.

*To whom correspondence should be addressed. Fax: +972-4832-5339; e-mail: adgold@netvision.net.il

2.2 Specimens

The basic specimen type was disc shaped [diameter (d) = 17 mm, height (h) = 4 mm] having been formed by cold isostatic pressing (CIP) at 200 MPa. Other simple shape specimens (d = 20 mm, h = 8, 12 mm; d = 23 mm, h = 4 mm; d = 11 mm, h = 11 mm) were also examined together with convex top cylinders (d = 15 mm, h = 15 mm). The green bulk density (BD_g) of the specimens was 46% of the theoretical density (44% t.d. for the convex top cylinders) assuming a theoretical density of 6·08 g cm^{-3}.[17]

2.3 Sintering

MW sintering was performed in two furnace types, which differ in relation to the electromagnetic field distribution pattern. The first type (model 10 of MMT, Knoxville, TN), allows concentration of the field in the central region of the applicator by suitably positioning antennae attached to the four magnetrons. The second system (model 101 of MMT) has a relatively large applicator (d = 90 cm, L = 137 cm) and includes a mode stirrer. These features markedly enhance *field distribution homogeneity* throughout the volume of the applicator.

The heating chamber set up, used in both furnaces, is shown in Fig. 1. The number of samples heated during a run varied between one and six. Conventional sintering was carried out in a tubular fast firing furnace in air. Heating schedules are referred to in Section 3.4. Temperatures were measured in all cases with S type thermocouples.

2.4 Characterization

The phase composition of the starting powder and sintered specimens was examined by XRD. Their microstructure was studied by electron microscopy (SEM) performed on specimens which underwent polishing and chemical etching. Density was measured by the Archimedes technique, using water as the immersion medium.

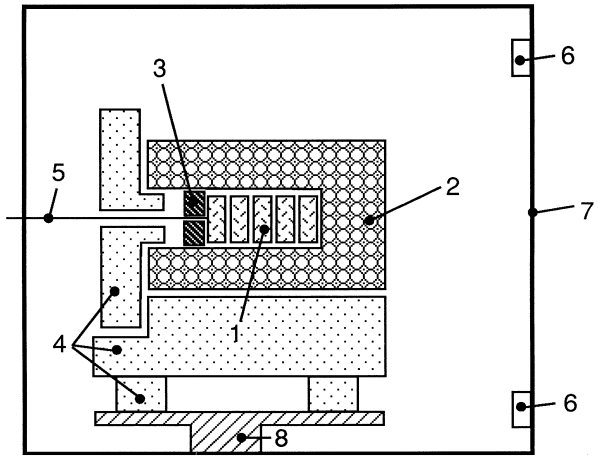

Fig. 1. Heating chamber configuration. 1, Specimens; 2, bubble alumina thermal insulation in sintered alumina container; 3, sintered alumina disc; 4, porous alumina parts providing thermal insulation; 5, Pt sheathed S-type thermocouple; 6, MW insertion points; 7, applicator wall; 8, metal stand.

The presence of cracks was determined by visual and optical microscopy inspection using fuchsin solution to enhance their visibility.

The bending strength of bars (3×4×15 mm) cut from conventional and MW sintered specimens was measured by three point bending using a span of 12 mm.[18] The tensile surface of the samples was polished up to a 0·25 μm finish. Fracture toughness was measured by a chevron notch technique. In all the tests crosshead speed was 50 μm/min^{-1}. A minimum of four samples was tested in each case in order to establish average values of bending strength and fracture toughness. Vickers hardness was measured using a load of 50 N with a duration of 15 s. To enhance the optical contrast, a thin layer of gold was deposited by sputtering on the polished surfaces of the specimens. An average hardness value was calculated using the results of 10 indentations.

3 Results and Discussion

3.1 Behaviour of ZrO_2 (Y_2O_3) during MW sintering

Results obtained by different authors, for the dielectric properties of zirconias, diverge considerably. Data given by Batt *et al.*[19] were considered below.

Substituted zirconias have a temperature profile of the dielectric loss factor which is different from those of other usual, oxide or non oxide, ceramics. At room temperature (RT) the imaginary part of the complex relative permittivity, ε'', of yttria-stabilized zirconias has values quite close to those exhibited by MW 'transparent' materials, like alumina or spinel ($\varepsilon''_{TZP} \sim 0{\cdot}04$). The loss factor increases markedly to $\varepsilon'' \sim 100$ around 1000°C ($\varepsilon''_{Al_2O_3} \sim 0{\cdot}3$ at the same temperature) to a level similar to that of conductive ceramics such as α-SiC.[19] At RT the loss is entirely due to polarization. The high value of the dielectric constant $\varepsilon' = 35$–40, suggests a significant contribution from $2Y'_{Zr} - V_0^{\cdot\cdot}$ dipoles because in monoclinic, pure, zirconia the dielectric constant has a lower value, $\varepsilon' \approx 13$, in the range expected considering only the ionic polarization of the oxide lattice. Over 500°C the contribution of the O^{2-} based ionic conductivity to the loss starts to be noticeable. The MW penetration depth in ZrO_2 (3 mol% Y_2O_3), at RT, of 2·45 GHz radiation (λ_0 = 122·4 mm)—calculated using the procedure proposed by Chabinsky[20] —is $D_p \sim 1{\cdot}5$ m. At 1200°C the D_p drops to ~1 mm.

The ε'' temperature profile suggests that strong MW/TZP interaction—and, as a consequence, heat

generation—may be expected over 500–600°C. The amount of heat generated cannot be estimated because the changes in porosity, during sintering, which are accompanied by a steep D_p reduction, continuously modify the fraction of the specimen's mass interacting with the MW. Initial heating of the material is expected to be sluggish ($\varepsilon'' < 1$ up to 400°C) and heating, during the last stages of densification, to be nonuniform due to the low D_p.

The low thermal conductivity of TZP, ~2 W/m°K, combined with a high thermal expansion ($\alpha = 10 \times 10^{-6}$/°K) suggest that thermal (or $m \rightarrow t$ related) stresses resulting from nonuniform and/or fast heating may cause warpage/cracking, especially in the case of large and/or low symmetry work pieces.

3.2 MW–HWS process

Various target load mass values and forward power profiles were examined. A minimal mass exists below which autoheating will not take place even at high MW forward power levels. For the case of the zirconia powder used (specific surface area of 22 m^2g^{-1}) and the specific insulation system configuration this mass was 10–12 g for forward power levels in the 1·5–2·0 kW region. It was observed that an efficient forward power profile requires a high power initial segment. If subsequently the power is suitably reduced, at temperatures over 500°C, *thermal runaway can be prevented* albeit quite fast temperature increase, in the 400–1000°C range, is unavoidable.

The optimal MW power profiles established allowed full sintering without cracking or warping. Figure 2 presents the temperature profiles, obtained in both the MMT 10 and MMT 101 applicators, when heating a 15 g load of TZP, under conditions, which determine full sintering (i.e. $BD_f \geq 99\%$ t.d.) at minimal peak temperature.

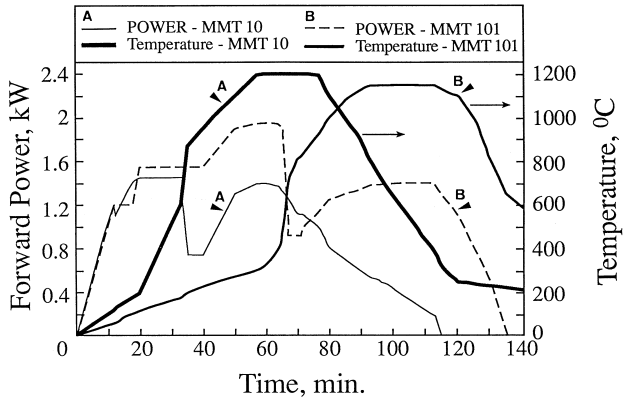

Fig. 2. Forward power and resulting temperature time profiles ensuring full densification of TZP at minimal peak temperatures. MMT 10 MW furnace, nonuniform MW field distribution with intensity enhancement in central region of applicator; MMT 101 MW furnace, uniform MW field distribution throughout the applicator's volume.

The different field distribution patterns and mean field-strength values, in the two applicators, determine noticeable differences in the temperature–time curves generated by a given forward power profile (see the first 30 min in Fig. 2). As a result the power profile required to reach a given peak temperature is different in the two MW furnaces examined. In the applicator exhibiting the more uniform field distribution and lower field strength (MMT 101) the interaction of the specimens with the MW is weaker at low temperature, but maximal densification is reached at somewhat lower temperatures than in the furnace which has the field concentrated in its central region (nonuniform field distribution).

It has been shown[4] that direct MW sintering of TZP is feasible in tuned *single mode cavities*. The results presented above show that it is also feasible in *multi-mode applicators* despite the low value of ε'' at room temperature. The heating process may be controlled so as to prevent specimens from cracking or warping. The sintering temperatures which were required when using the approach of Tian *et al.*,[4] could be reduced by some 400°C by optimizing heating schedules.

3.3 Sintering in nonoxidizing atmosphere

The structure of TZP sintered in air is not identical to that obtained in oxygen deficient atmosphere. Under N_2 some Zr^{3+} (d^1 ion) may form by partial reduction of Zr^{4+}. Oxygen loss according to the process $O_0 \Longleftrightarrow V_0^{\cdot\cdot} + 2e' + 1/2O_2$ may create V_0 type point defects. A more drastic reductive process would generate Zr^0 atoms, which may agglomerate in colloidal size particles. Such defects absorb or scatter visible light and are also likely to influence the dielectric properties, especially at high temperature. The black colour acquired by the specimens indicated that defects are formed indeed during their MW heating in nitrogen.

Schedules similar to those used in air produce—when heating is done under nitrogen—the same levels of densification. It seems that the defects, which form under N_2, do not noticeably influence the TZP's interaction with the MW fields. Annealing over 1250°C in air eliminates the black colour induced by the processing under nitrogen.

3.4 Comparison of MW and conventional sintering

In Table 1 the densification levels obtained for various peak temperatures in the MMT 10 furnace are presented for the case of a 20 min dwell time, at peak temperature, and a mean heating rate of 12°C min^{-1} (at temperatures higher than 800°C). The densification levels (BD_f) obtained in the MMT 101 (8°C/min^{-1} at temperatures higher than 600°C) and, respectively, a conventional furnace

Table 1. Densification of the zirconia powder compacts, after various heating schedules, in MW and conventional furnaces

Sintering temperature (°C)	*Bulk density (% of t.d.)*			
	MW			*Conventional*[a]
	MMT 10 A[a]	*MMT 101*[a]	*MMT 10 B*[b]	
1100	94·4	98·3	—	80·0
1170	97·5	99·0	—	82·0
1200	99·0	99·5	—	94·0
1250	99·5	99·5	—	97·0
1300	99·5	99·5	98·0	98·4
1350	99·5	99·5	—	99·3
1400	99·5	—	98·3	99·3
1500	—	—	99·0	99·1
1600	—	—	—	95·5
1700	—	—	—	94·0

[a]Dwell time at peak temperature was 20 min; heating rates $\sim 10°C\,min^{-1}$.
[b]No dwell time at peak temperature; heating rate $100°C\,min^{-1}$.

($12°C\,min^{-1}$, from RT) for the same dwell time are also shown.

For the case of the MMT 10 furnace results obtained by fast firing at $\sim 100°C\,min^{-1}$ (no dwell time at peak temperature) are also presented.

In all fully sintered specimens monoclinic zirconia was absent, despite the quite high content of this phase present in the initial powder. The XRD pattern of a sintered specimen and that of the initial powder are shown in Fig. 3. In the 72–75° range of the XRD pattern only the (004)t and (400)t peaks were observed indicating the absence of cubic phase.

Preliminary thermal treatments to eliminate volatiles and/or convert monoclinic residue to tetragonal crystals were found necessary by some authors[4,7] in order to obtain uncracked specimens. No such processing was required here.

As the data in Table 1 shows, enhancement of the sintering rate is obtained under the influence of the MW field. In the MW furnace 98·3% t.d. was attained as low as 1100°C (MMT 101). Similar density required heating to 1300°C in the resistive furnace. The maximal BD_f of 99·5% t.d. was obtained *reproducibly* at temperatures $\geq$1250°C (in many cases also at 1200°C), in the MW furnaces. In the conventional furnace BD_f >99% t.d. was obtained for temperatures of at least 1350°C. As it may be observed differences in the densification level—between the MW and resistive furnace fired specimens—were noticeable in the 1100–1300°C domain gradually disappearing at higher temperatures. Contrary to the results obtained by other workers[4,11] in the case of zirconia sintering a 'MW effect' is maintained until the completion of densification, in accord with the findings of Janney *et al.*[6] The effect is stronger at lower densification levels. Accelerated diffusion, especially of O^{2-} ions,

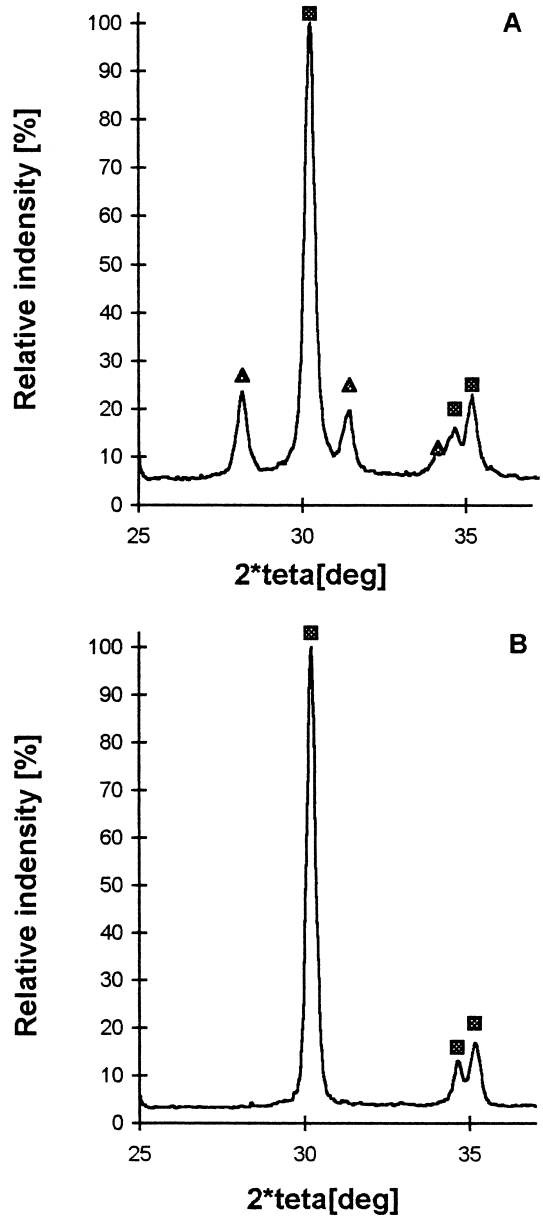

Fig. 3. XRD patterns of TZP: A, as-received powder; B, specimen after MW sintering, in air, at 1200°C 20 min. ■, Tetragonal phase; ▲, monoclinic phase.

seems to be the cause of the increase in TZP sintering rate brought about by exposure to MW fields.[14,21] In conventional furnaces full sintering at temperatures $\leq$1300°C was previously obtained only in the case of ZrO_2 (Y_2O_3) powders lacking agglomerates or having *very soft* ones.[22–24] Here, in the MW furnace, the same result is obtained also for the case of commercial powders—which exhibit multilevel strong aggregates—without applying any special processing.

The differences in overall heating time (same dwell time at peak temperature), between furnaces MMT 10 and 101, did not influence the maximal densification level achievable. On the other hand, in the more uniform field of MMT 101 somewhat lower temperatures are required for a given level of densification.

The cracking propensity of the specimens (which attained $BD_f \geq 98\%$ t.d.) was a function of size and green specimen *densification uniformity*. Table 2 shows the yield in uncracked pieces when heating various types of specimens (MMT 101; 8°C min^{-1}; 20 min at peak temperature). It is believed that marked yield improvements in the case of large and/or complex shape specimens can be attained if heating cycles adapted to each particular specimen type are employed.

The ultrafast firing, at ~100°C min^{-1} (see Table 1), while permitting full densification after very short heating cycles always generated cracked specimens.

In Fig. 4 various green and MW sintered specimens are shown.

3.5 Microstructure of sintered specimens

Equiaxed grains were observed in the SEM pictures of the specimens sintered either by MW–HWS or CFH. The structure of the strong agglomerates, present in the powder is preserved, to a large extent, in the fired bodies. The microstructure of a specimen MW sintered at 1300°C ($BD_f = 6{\cdot}03$ g cm^{-3}) is shown in Fig. 5 together with that of the initial zirconia powder.

Grain size remained submicron at all temperatures, up to 1500°C, abnormal grain growth being virtually absent.

No significant differences—regarding the grain size distribution—were observed between the MW and conventionally fired specimens.

Table 2. Yield in uncracked specimens (MW sintering) as a function of their size and shape

Specimen type	d = *17 mm*; h = *4 mm*	d = *11 mm*; h = *11 mm*	d = *23 mm*; h = *4 mm*	*Convex top cylinders*
Yield (%)	85	85	40	15

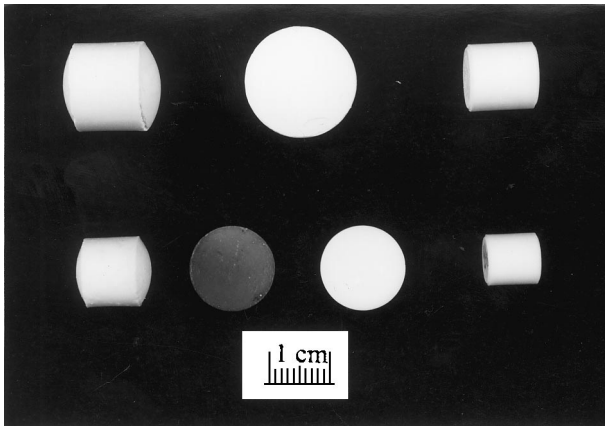

Fig. 4. Various shape specimens before and after MW sintering: upper row, green parts; lower row, MW sintered parts (1300°C 20 min); black disc was sintered, under N_2 (1200°C).

3.6 Mechanical properties

For comparison purposes measurements were made on specimens densified by MW–HWS or CFH at 1350°C. At this sintering temperature both specimen types were fully dense. Results regarding the bending strength, the fracture toughness (as expressed by K_{IC}) and Vickers hardness data are presented in Table 3. The MW and conventionally fired specimens exhibit similar mechanical properties. For the case of the MWed specimens the values measured on specimens sintered at 1200°C were similar to the values measured on those fired at 1350°C. In the case of specimens conventionally sintered at 1200°C marked fluctuations from

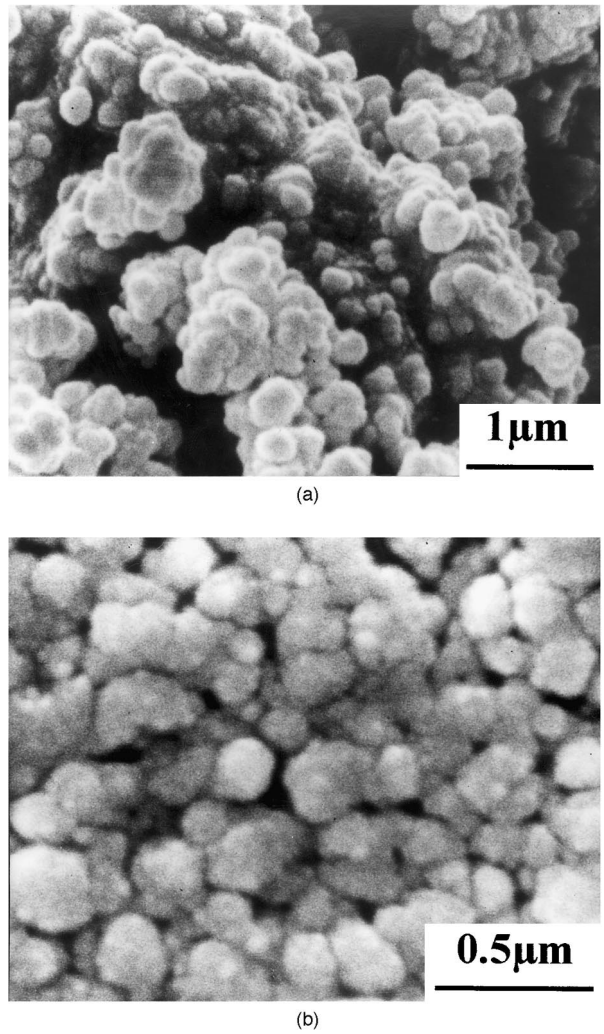

Fig. 5. Microstructure of initial TZP powder and sintered specimen ($BD_f = 6{\cdot}03$ g cm^3). SEM pictures: (a) TZP powder; (b) sintered specimen: 1300°C 20min in air (cross section, polished and chemically etched).

Table 3. Mechanical properties of ZrO_2 specimens microwave and conventionally sintered at 1350°C 20 min

Sintering approach	*BD_f (% of t.d.)*	*Bending strength (MPa)*	*K_{IC} (MPa m$^{1/2}$)*	*Hardness (kg mm^{-2})*
CFH	99·3	610 ± 31	5·61 ± 0·2	1435 ± 25
MW–HWS	99·5	637 ± 43	5·76 ± 0·35	1451 ± 33

specimen to specimen were observed—probably due to the still large residual porosity—precluding comparison with the MWed specimens.

4 Conclusions

If suitable MW (2·45 GHz) power-time profiles are employed—and correlated with the mass of the target load—it is possible to heat, starting from room temperature, ZrO_2 3 mol% Y_2O_3 powder compacts up to the temperatures required for full sintering *without using susceptors*, in MW powered furnaces having *multimode* applicators. Thermal runaway may be prevented and heating curves exhibiting desired peak temperatures and dwell times, at maximal temperature, can be obtained. Fully sintered, uncracked, parts can be produced at temperatures as low as 1200°C (15–20 min dwell times) at heating rates (over 500°C) $\geq 10°C\,min^{-1}$. A noticeable increase of the sintering rate is brought about by the use of the MW powered furnace instead of a resistive one, minimal temperatures required for full sintering (for a given dwell time) being reduced. Cracking propensity is a function of size and green densification uniformity. Currently only small size workpieces can be produced with a yield in uncracked specimens acceptable for practical applications. Heating under oxygen-free atmospheres does not noticeably influence the MW sintering process despite modifications induced in the point defects system existent in the TZP's lattice.

References

1. Blake, R. D. and Meek, T. T., Microwave processed composite materials. *J. Mat. Sci. Lett.*, 1986, **5**, 1097–1098.
2. Meek, T. T., Holcombe, C. E. and Dykes, N., Microwave sintering of some oxide materials using sintering aids. *J. Mat. Sci. Lett.*, 1987, **6**, 1060–1062.
3. Wilson, J. and Kunz, S. M., Microwave sintering of partially stabilized zirconia. *J. Am. Ceram. Soc.*, 1988, **71**, C40–C41.
4. Tian, Y. L., Li, B. S., Shi, J. L., Xu, Y. P., Guo, J. K. and Yen, D. S., Microwave sintering of Y_2O_3(3%)–ZrO_2(TZP). In *Proceedings of the Symposium Microwaves: Theory and Application in Materials Processing*, Cincinnati, OH, 29 April–3 May 1991, ed. D. Clark, F. Gac and W. Sutton. ACerS, Westerville, OH, 1991, pp. 577–584.
5. Samuels, J. and Brandon, J. R., Effect of composition on the enhanced microwave sintering of alumina-based ceramic composites. *J. Mat. Sci.*, 1992, **27**, 3259–3265.
6. Janney, M. A., Calhoun, C. L. and Kimrey, H. D., Microwave sintering of solid oxide fuel cell materials: I, zirconia–8 mol%–yttria. *J. Am. Ceram. Soc.*, 1992, **75**, 341–346.
7. Kim, D. H. and Kim, C. H., Entrapped gas effect in the fast firing of yttria-doped zirconia. *J. Am. Ceram. Soc.*, 1992, **75**, 716–718.
8. Janney, M. A., Jackson, M. L. and Kimrey, H. D., Microwave sintering of ZrO_2–12 mol% CeO_2. In *Proceedings of the Symposium Microwaves: Theory and Application in Materials Processing II*, Cincinnati, OH, 19–22 April 1993, ed. D. Clark, W. Tinga and J. Laia, Jr. ACerS, Westerville, OH, 1993, pp. 101–107.
9. Zhang Jinsong, Yang Yongjin, Cao Lihua, Microwave sintering of nanocrystalline ZrO_2 powders. In *Materials Research Society Symposium Proceedings*, Vol. 347, ed. M. Iskander, R. Lauf and W. Sutton. Mat. Res. Soc., Pittsburgh, PA, pp. 591–596.
10. Wroe, F. C. R. and Rowley, A. T., Microwave enhanced sintering of ceramics. In *Proceedings of the Symposium Microwaves: Theory and Application in Materials Processing III*, Cincinnati, 1–3 May 1995, ed. D. Clark, D. Folz, J. Oda and R. Sieberglitt. ACerS, Westerville, OH, 1995, pp. 69–76.
11. Nightingale, S. A., Worner, H. K. and Dunne, D. P., Microstructural development during the microwave sintering of yttria–zirconia ceramics. *J. Am. Ceram. Soc.*, 1997, **80**, 394–400.
12. Setsuhara, Y., Kamai, M., Kinashita, S., Abe, N., Miyaki, S. and Saji, T., Advanced ceramics sintering using high-power millimeter-wave radiation. In *Materials Research Society Symposium Proceedings*, Vol. 430, ed. M. Iskander, J. Kiggans and J. Bolomey. Mat. Res. Soc., Pittsburgh, PA, pp. 533–538.
13. Saji, T., Microwave sintering of large products. In *Materials Research Society Symposium Proceedings*, Vol. 430, ed. M. Iskander, J. Kiggans and J. Bolomey. Mat. Res. Soc., Pittsburgh, PA, pp. 15–20.
14. Janney, M. A. and Kimrey, H. D., Diffusion-controlled processes in microwave-fired oxide ceramics. In *Materials Research Society Symposium Proceedings*, Vol. 189, ed. W. B. Snyder, W. H. Sutton, M. F. Iskander and D. Lynn Jhonson. Mat. Res. Soc., Pittsburgh, PA, pp. 215–227.
15. Iskander, M., Computer modeling and numerical simulation of microwave heating systems. *MRS Bulletin.*, 1993, **18**, 30–36.
16. Srivastava, K. K., Patil, R. N., Chaudhary, C. B., Gorkhale, K. V. G. and Subbarao, C. E., Revised phase diagram of the system ZrO_2–$YO_{1·5}$. *Transactions and Journal of the British Ceramic Society*, 1974, **73**, 85–91.
17. Ingel, R. P. and Lewis, III, D., Lattice parameters and density for Y_2O_3-stabilized ZrO_2. *J. Am. Ceram. Soc.*, 1986, **69**, 325–332.
18. Shannon, J. L. and Munz, D., Specimen and geometry effects on fracture toughness of aluminum oxide measured with short-rod and short bar Chevron-notch specimens: testing and analysis. *ASTM STP*, 1984, **855**, 270–280.
19. Batt, J., Binner, J. G. P., Cross, T. F., Greenacre, N. D., Hamlyn, M. G., Hutceon, R. M., Sutton, W. H. and Weil, C. M. In *Proceedings of the Symposium Microwaves: Theory and Application in Materials Processing III*, Cincinnati, 1–3 May 1995, ed. D. Clark, D. Folz, J. Oda and R. Sieberglitt. ACerS, Westerville, OH, 1995, pp. 243–250.
20. Chabinsky, I. J. and Eves, III, E. F., The application of microwave energy in drying, calcining and firing of ceramics. *Interceram.*, 1986, **6**, 30–37.
21. Janney, M. A., Kimrey, H. D., Allen, W. R. and Kiggans, J. O., Enhanced diffusion in sappire during microwave heating. *J. Mat. Sci.*, 1997, **32**, 1347–1355.
22. Rhodes, W. H., Agglomerate and particle size effects on sintering yttria-stabilized zirconia. *J. Am. Ceram. Soc.*, 1981, **64**, 19–22.
23. van de Graaf, M. A. C. G., and Burggraaf, A. J., Wet-chemical preparation of zirconia powders: their microstructure and behaviour. In *Proceedings of the 2nd Intl. Conf. on the Science and Technology of Zirconia*, ed. N. Claussen, M. Rhule and A. Heuer. ACerSoc, Columbus, OH, 1984, pp. 744–765.
24. Sagel-Ransijn, C. D., Winnubst, A. J. A., Burggraaf, A. J. and Verweij, H., Grain growth in ultrafine-grained Y-TZP ceramics. *J. Eur. Ceram. Soc.*, 1997, **17**, 1133–1141.